ACS OMEGA

http://pubs.acs.org/journal/acsodf

Article

High-Throughput Screening of 3D-Printed Architected Materials Inspired by Crystal Lattices: Procedure, Challenges, and Mechanical Properties

Maxim Yu. Arsentev,* Evgeny I. Sysoev, Alexey I. Makogon, Sergey V. Balabanov, Maxim M. Sychev, Mahmoud H. Hammouri, and Vyacheslav A. Moshnikov

Cite This: *ACS Omega* 2023, 8, 24865−24874

Read Online

ACCESS | Metrics & More | Article Recommendations | Supporting Information

ABSTRACT: The search for load-bearing, impact-resistant, and energy-absorbing cellular materials is of central interest in many fields including aerospace, automotive, civil, sports, packaging, and biomedical. In order to achieve the desired characteristic geometry and/or topology, a perspective approach may be used, such as utilization of atomic models as input data for 3D printing of macroscopic objects. In this paper, we suggest a new approach for the development of advanced cellular materials—crystallomorphic design based on selection of perspective crystal structures and modeling of their electron density distribution and utilization of isoelectronic surfaces as a generatrix for 3D-printed cellular materials. The ATLAS database, containing more than 10 million existing and predicted zeolites, was used as a source of data. Herein, we introduced a high-throughput screening of a data array of crystalline compounds. Several perspective designs were identified, implemented by 3D printing, and showed high characteristics. A linear correlation was found between the strength of the samples and the minimum angle and minimum bond length in the simplified crystal structures. A new cellular geometry with reinforcement struts and increased strength was discovered. This property was found by us independent of the other works, in which the cellular structures were developed by an explicit method. Thus, the developed approach holds perspective for the design of new cellular structures with increased characteristics and for the prediction of their properties.

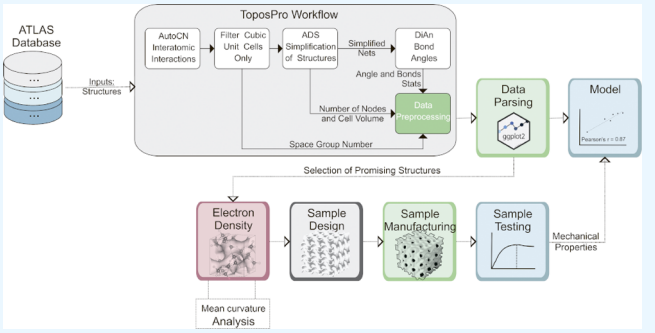

1. INTRODUCTION

Cellular materials with low weight have a number of interesting properties, such as high specific strength, rigidity, and large compaction deformations, which make these materials promising in various engineering problems. For example, cellular structures are used in protective structures,[1] heat exchangers,[2] highly loaded load-bearing structures, and biomedical implants.[3,4]

In some cases, the desired mechanical response is achieved by changing the composition of the material. Other possible routes are inspired by nature, where geometry and/or topology determine most of the observed mechanical properties, such as bones,[5] sea shells,[6] ladybug feet,[7] shark teeth,[8] woodpecker endoskelet,[9] and beaks of a kingfisher.[10] However, geometry-controlled structures are not easy to reproduce due to the lack of appropriate synthesis methods. Recent advances in additive manufacturing (AM) techniques have paved the way toward the efficient fabrication of complex geometries.[11−19]

In the works of Shevchenko, it was shown that structures based on triply periodic minimal surfaces (TPMS) are superior in the conditions of extreme mechanical loading due to their physical nature.[20,21]

TPMS are a class of mathematically defined surfaces that exhibit 3D periodicity and zero mean curvature and are composed of repeating elements with the smallest possible area. The Fermi surfaces of metals and equipotential surfaces are important examples of minimum energy thrice-periodic surfaces. Nature gives many examples of labyrinth geometries based on thrice-periodic surfaces of minimum energy. For example, in the wings of *Callophrys rubi* butterflies, chitin is organized in the form of a gyroid, where it functions as a photonic crystal to scatter light and create a characteristic iridescent appearance.[22]

The formation of structures with the TPMS geometry in lipid−water systems,[23] synthetic surfactants,[24] alveolar structures of rabbit lungs,[25] and in inorganic mesoporous systems

Received: February 10, 2023
Accepted: June 26, 2023
Published: July 6, 2023

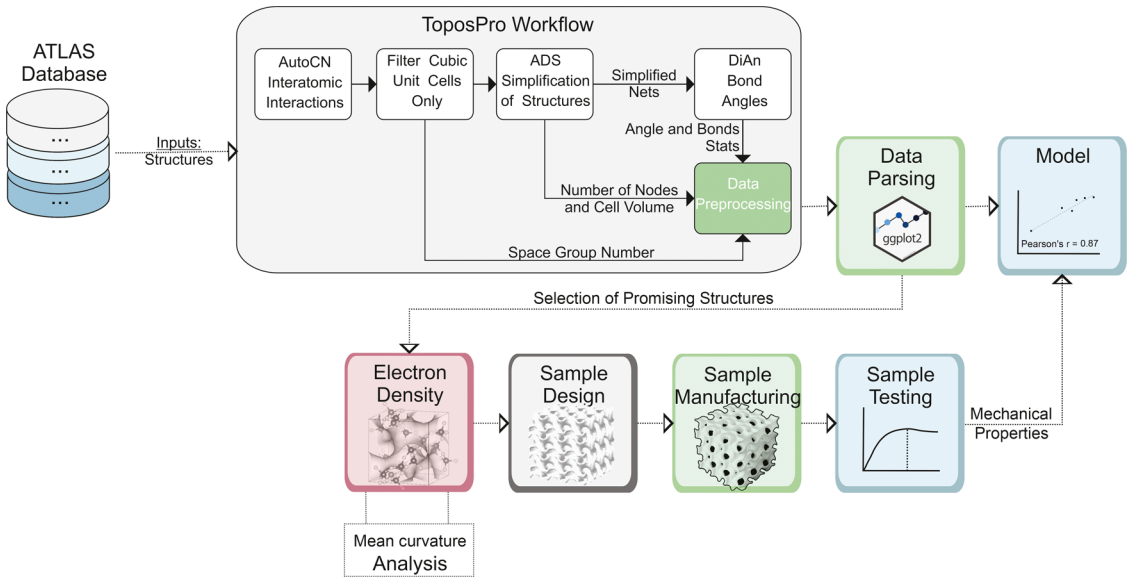

Figure 1. Algorithm of the crystallomorphic design of new cellular structures.

synthesized in the presence of amphiphilic components[26] has been shown.

Von Schnering in his early work[27] showed the existence of TPMS in crystals of a certain symmetry as a surface of zero potential. The analysis of literature sources showed that there are only a few publications on the presence of TPMS in the structures of zeolites. For example, in,[28] the formation of gyroid channels was experimentally observed. In,[29] the authors showed that decorated carbon with a zeolite template divides space into two nonintersecting labyrinths that describe a three-times periodic minimum energy surface.

Due to good mechanical properties, recently, there have been a number of publications on TPMS-based materials. At the same time, a number of known TPMS are quite small, and in order to further develop these fields, scientists need new perspective TPMS-like geometries. Since well-known 3D structures are crystal ones, atomic models as inputs for 3D printing of macroscopic structures may be used.[19,30−34] The surface is obtained by interpolating all of the positions of the atoms and creating a mesh, which is subsequently used as input for the manufacture of 3D printing. Some 3D-printed structures have been found to have excellent mechanical performance in uniaxial compression and ballistic impact while being extremely lightweight.[35] This opens up new perspectives for applications that require strong and lightweight materials in structural applications such as aircraft and spacecraft. In particular, schwartzites[36] and tubulanes[35] are two families of carbon-based materials that have demonstrated the effectiveness of the concept of atomic 3D-printed structures mentioned above. Schwarzites are three-dimensional crystalline materials resembling triply periodic minimal surfaces (TPMS) in shape.[37] These are three-dimensional porous solids with periodic minimal surfaces having a negative Gaussian curvature, which can have unusual mechanical and electronic properties. The results show that these structures have great prospects as load-bearing and impact-resistant materials due to the unique lamellar deformation mechanism that occurs in these structures during loading.[36] Tubulanes are also three-dimensional crystalline structures based on cross-linked carbon nanotubes.[38] Recent studies have shown that many of the features observed in molecular dynamics (MD) simulations of carbon-based schwarcites and tubulanes are translated into their respective 3D-printed structures.[35,36,39] In particular, tubulanes have incredible ballistic impact characteristics when a high-velocity projectile stops at a depth of 5 mm in one of the studied 3D-printed structures.[35] Schwarzites and tubulanes also share a common feature: they have a cellular or porous structure, which makes them potential options for structural purposes.[40,41] Additionally, the deformation mechanisms and behavior at high strength are similar for atomic and 3D-printed macroscopic architected materials.[36] Hence, other porous structures with cavities may be of interest: zeolites, organic framework structures, crystalline sorbents, metal−organic frameworks (MOFs), porous polymer groups, and frameworks of ionic conductors. The use of the Atlas of Prospective Zeolite Structures (ATLAS) database,[42] containing more than 10 million predicted porous zeolite structures, opens up prospects for obtaining a diverse array of surfaces. In this work, we use topology generation based on the construction of isoelectronic surfaces for crystal structures available in the ATLAS database.

In this paper, we suggest a new approach for the development of new cellular structures—crystallomorphic design based on the selection of perspective crystal structures, modeling of their electron density distribution, and utilization of isoelectronic surfaces as a generatrix for 3D-printed cellular material. Herein, we introduce a high-throughput screening approach consisting of analysis of a data array of crystalline compounds and surfaces based on them. Further, we demonstrated correlations between basic crystallochemical data of simplified crystal structures and curvature of generated surfaces with mechanical properties of 3D-printed functional cellular materials.

2. MATERIALS AND METHODS

In this work, the ATLAS[42] database was used to create cellular materials.

As an alternative path, researchers use a range of methods, from intuitive to fully computerized, e.g., a method based on splitting the zeolite structure into sheets or blocks and assembling new zeolite structures based on them,[43] using an annealing simulation algorithm,[44] as well as machine learning

https://doi.org/10.1021/acsomega.3c00874
ACS Omega 2023, 8, 24865−24874

Table 1. Samples, Distinguished by Corresponding Sample IDs from the ATLAS[42] Database

sample	sample ID from ATLAS[42] database	space group (s.g. #)	number of Si atoms	lattice parameter (a, nm)
200	tmp_200_2_776_pPPlW0	$Pm\bar{3}$ (200)	8	9.781
202	tmp_202_2_31854_FTWU7K	$Fm\bar{3}$ (202)	32	13.415
208	tmp_208_1_231_3tBAji	$P4_232$ (208)	8	7.675
214	tmp_214_1_2241_eeU6n9	$I4_132$ (214)	12	9.739
221	tmp_221_1_1_3sg5b9	$Pm\bar{3}m$ (221)	48	14.835
222	tmp_222_2_1_1331_4vfhyH	$Pn\bar{3}n$ (222)	12	8.968

methods.[45] However, for the most accurate study, it is important to have a complete database containing all possible structures of zeolites based on all possible combinations of atomic arrangements in a unit cell. It is this combinatorial approach that is partially implemented in the ATLAS database.[42] It should be noted that in our work, only cubic crystal structures from the database were considered for analysis.

The high-throughput screening approach followed in this study is represented as a schematic in Figure 1, where four phases are highlighted: extraction of files from the database; simplification of structures; their crystal chemical analysis; generation of surfaces based on structure files and analysis of their curvature; sample design; sample manufacturing; sample testing; and numerical simulations.

2.1. Methods for the Analysis of Inorganic Crystalline Compounds. Using the ATLAS database, an array of cubic zeolite compounds was obtained, consisting of 279687 structures. The array was processed and sorted according to the number of nodes (1−6) belonging to the same elementary cell and space group. A statistical diagram of the distribution of structures is shown in Figure S1 (Supporting materials).

The complexity of calculating and rendering the electron density isosurface is related to the number of atoms in the cell (Figure S1). With an increase in the number of atoms, the area of the isosurface increases proportionally. This property of the studied objects directly follows from eqs 1 and 2. This ultimately leads to an increase in the size of the grid, which plays a key role in the computer-aided design (CAD) system. Because of this, it was decided to analyze structures with only 1−4 Si atoms (first selection).

The task of the analysis is to obtain a data array, which includes information about the space group of the compound; the number of silicon atoms (number of nodes); the number of bonds; the unit cell volume; the maximum, minimum, and average value of the bond length between atoms; and the maximum, minimum, and average value of the angle between silicon atoms. For automated search, sorting, structure simplification, and crystallographic analysis of zeolites, the ToposPro[46] software package, a program for geometric and topological analysis of crystal structures, was used.

The analysis process begins with the import of zeolite database files in the Crystallographic Information File (CIF) format. Then, within the framework of the task, three modules were used (AutoCN, ADS, Dian) (the detailed description is presented in the Supporting Materials, section "Crystal chemical structure analysis using ToposPro"). Our methodology here is based on considering simplified structures as they ultimately determine the shape of the isoelectronic density and the 3D model for printing.

One sample from each space group (six in total) was selected and analyzed (Table 1). For convention, we will assume that the sample number corresponds to the space group number. Information on the number of atoms and the volume of the unit cell, the number of bonds, the length of bonds, and the values of the angles between atoms were extracted (Table S1). For statistical data processing of a large number of structures, a script written using R programming language[47] was developed.

2.2. Method of Modeling of the Surface. When modeling cellular structures, the method of "crystallomorphic design" was used, the main stages of which are shown in Figure 2.

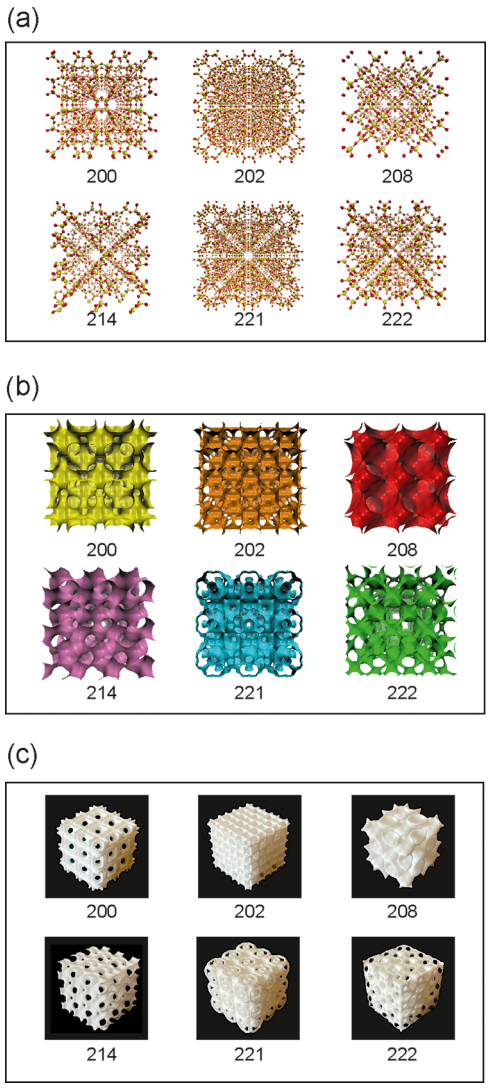

Figure 2. Process of "crystallomorphic design": (a) original crystalline 3 × 3 × 3 supercells (200, 202, 208, 214, 221, 222), (b) CAD model of electronic density, (c) 3D-printed samples.

https://doi.org/10.1021/acsomega.3c00874
ACS Omega 2023, 8, 24865−24874

We considered two approaches to obtain isoelectronic density distribution. The first one, which is more accurate, but requiring large computing power, is based on the application of the density functional theory (DFT).[48,49] The second approach, fundamentally different and less accurate, is based on the Fourier transform of the structure factors $F(h)$, which are calculated from the structure parameters and atomic scattering factors of free atoms using VESTA software.[50] In X-ray diffraction, the reflectance structure factor F with diffraction indices hkl is formulated as

$$F(h) = \sum_{j=1}^{n} g_j f_j(h) T_j(h) \exp[2\pi i(hx_j + ky_j + lz_j)] \quad (1)$$

where n is the total number of atoms in a unit cell, j is the index of the atom, g_j is the coefficient filling (settlement), $f_j(h)$ is the atomic form factor, $T_j(h)$ is the Debye−Waller factor, and x_j, y_j, and z_j are the atomic coordinates. For the studied compounds, the difference between the methods is insignificant, so calculation of the electron density was carried out using VESTA software.[51]

When calculating the density, it is necessary to set the resolution in units of Å. The resolution sets the number of grid nodes N along each crystallographic axis in such a way that the distance between each node is close to the set value. The electron density ρ is determined at each point (x, y, z) in the entire volume of the unit cell V by the formula

$$\rho(x, y, z) = \frac{1}{V} \sum_{h=-N_x/2}^{N_x/2} \sum_{k=-N_y/2}^{N_y/2} \sum_{l=-N_z/2}^{N_z/2} F(h) \exp [2\pi i(hx + ky + lz)] \quad (2)$$

The described method is implemented in the VESTA software package,[51] which allows one to visualize the structure and three-dimensional grids, such as electron/nuclear densities.

2.3. Adding Shell Thickness. Regardless of the method used to calculate the electron density, the visualization of the isoelectronic surface was carried out in VESTA. In the stereolithography (STL) format, the model was exported and imported into Rhinoceros CAD, where the Offset Mesh tool was used, which set the indent of the original polygonal mesh to 0.4 mm in both directions, which leads to the creation of a wall with a thickness of 0.8 mm.

2.4. Sample Manufacturing and Printing Parameters. Selective laser sintering (SLS technology) was used for 3D printing of samples as it is a high-throughput high-quality process, which is the most frequently used in the industry for structural parts. Printing was carried out on the EOS Formiga P110 machine. The polyamide-12 (PA2200, PA12) polymer was used due to its high elastic and plastic properties. Printing conditions were as follows: height of the layer: 100 μm; table temperature: 169.5 °C; camera temperature: 150 °C. To determine the elastic and plastic properties of the material, cylinders were tested in accordance with ISO 604:2002 Tables 2 and 3.

2.5. Mechanical Testing. The samples were tested for compressive strength on a universal testing machine Shimadzu AG-50kNXD at an air temperature of 25 °C and a loading speed of 5 mm/min in accordance with ISO 604:2002 "Plastics—Determination of compressive properties". It is known that 3D-printed products are characterized by high anisotropy that occurs due to the layered construction of samples. In this regard, the tests were carried out along the growth axis (along the z-axis).

Table 2. Linear Mechanical Properties of 3D-Printed Polyamide-12

density (g/cm^3)	Young's modulus (MPa)	Poisson's ratio	yield strength (MPa)	compressive strength (MPa)
1.00	1440	0.33	27	44

To assess the prospects of using designed samples as energy absorbers, the characteristics were analyzed according to.[52]

The damping characteristic of cellular materials in the form of impact absorption energy A from stress−strain curves was calculated as

$$A = \int_0^{\varepsilon_{max}} \sigma d\varepsilon \quad (3)$$

where ε_{max} and σ_{max} are the maximum deformation before the beginning of the compaction area and the stress of the ultimate strength of the sample, respectively.

The effective impact absorption energy E'' can be calculated as

$$E' = \left(\int_0^{\varepsilon_{max}} \sigma d\varepsilon\right) / (\sigma_{max}\varepsilon_{max}) \quad (4)$$

where σ_{max} is the maximum stress achieved during the test of the samples in sections of linear and elastoplastic deformation on the stress−strain curve.

2.6. Surface Curvature Measurement Methods. To measure the curvature of surfaces, a script was developed and used (Supporting Information), which allows one to find the minimum, maximum, Gaussian, and mean curvature of the model's surface. According to Alain McKay, TPMS-based structures are capable of dissipating mechanical energy quite efficiently.[14,53−56] One of the most important properties of TPMS, which provides them with high mechanical properties, is the zero mean curvature.[2,57] The mean curvature of a surface is an extrinsic measure that comes from differential geometry and that locally describes the curvature of an embedded surface.[58] Thus, it can be assumed that structures with mean curvature values tending to 0 have better mechanical properties.

The script allows one to display the distribution of the mean curvature on the surface in the form of a color map, which can be used to determine areas of a sharp change in magnitude.

3. RESULTS AND DISCUSSION

3.1. Results of Crystallographic Structural Analysis. As a result of crystallographic analysis, about 39 000 structures were processed. As mentioned in Section 1, the structural diversity of the zeolite structures is so large that for the convenience of maintaining statistics, one can use the so-called counting diagram: namely, the point size on such types of graphs indicates the number of structures with the same value along the y-axis (Figure 3). This graph was generated using *Ggplot2*,[47] a data visualization package for the statistical R programming language.

The main criteria by which candidates for the study of mechanical properties were selected were the number of nodes in the simplified structures (the detailed description is presented in the Supporting Materials, section "Crystal

https://doi.org/10.1021/acsomega.3c00874
ACS Omega 2023, 8, 24865−24874

Table 3. Nonlinear Mechanical Properties of 3D-Printed Polyamide-12

true stress (MPa)	27.12	30.00	34.09	37.00	40.01	43.02	46.00
true plastic deformation	0	0.002	0.007	0.011	0.016	0.023	0.032

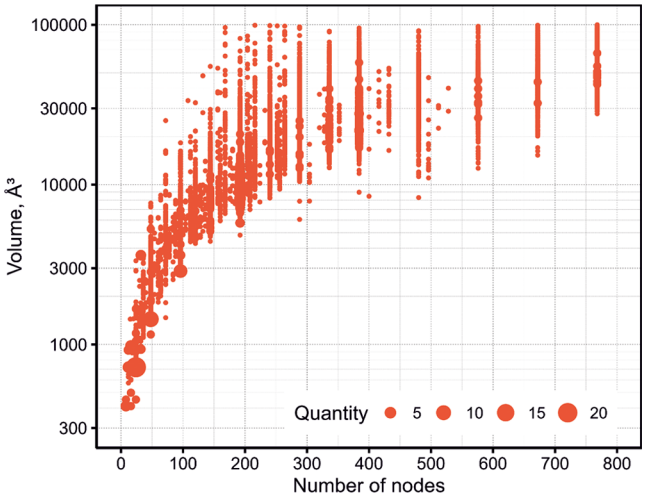

Figure 3. Relationship between the number of nodes of the simplified structure and cell volume.

chemical analysis using ToposPro") and the cell volume. Figure 3 shows the statistics of these parameters.

Information on the statistics of other structure parameters, such as maximum, minimum, and average values of bond length and angle between bonds in the simplified structures, may be found in the Supporting Information (Table S1).

3.2. Results of Rapid Screening of Crystal Structures. It was found that crystalline compounds of zeolites from different space groups could form the same isotype structure. This is due to the peculiarity of database generation, which does not take into account all sorts of permutations, shifts, and transfers.

Many zeolite frameworks with gyroid channels have been found. Since the isoelectronic density follows the shape of the channels, this leads to the fact that many different structures give the same TPMS-like gyroid geometry.

In spite of the fact that in ref 59 for the Schoen gyroid the corresponding TPMS-forming crystalline materials were not found, such a surface can be easily obtained on the basis of zeolites with gyroid channels, both from experimental structures and from theoretically predicted ones, which is demonstrated in this work.

This observation shows that, as a result of studying the extensive crystal databases, it is possible to find structures that make it possible to generate all known TPMS, and moreover, new TPMS-like surfaces may be founded.

Due to the presence of a large number of chemical restrictions, many structures are nevertheless eliminated.

Since only structures with a unique geometry are of the greatest interest, six compounds were selected from all cubic space groups, whose isosurfaces were not similar to each other.

The results of the computational screening are presented in the Supporting Information, along with the parameters of crystalline compounds.

The 214 and 200 space group isoelectronic surfaces are gyroid- and IWP-like (types of TPMS geometries), respectively. The structure 208 of the group forms two interpenetrating, without intersection, surfaces, so only one of them was used for 3D printing. Further, the designation of the sample corresponds to its spatial group.

3.3. Mechanical Testing of 3D-Printed Cellular Materials. 18 samples were printed with a TPMS-like topology, three for each surface under study. Deformation curves and specific strength of the 3D-printed samples are shown in Figure 4. The parameters of 3D-printed samples are shown in Table 4.

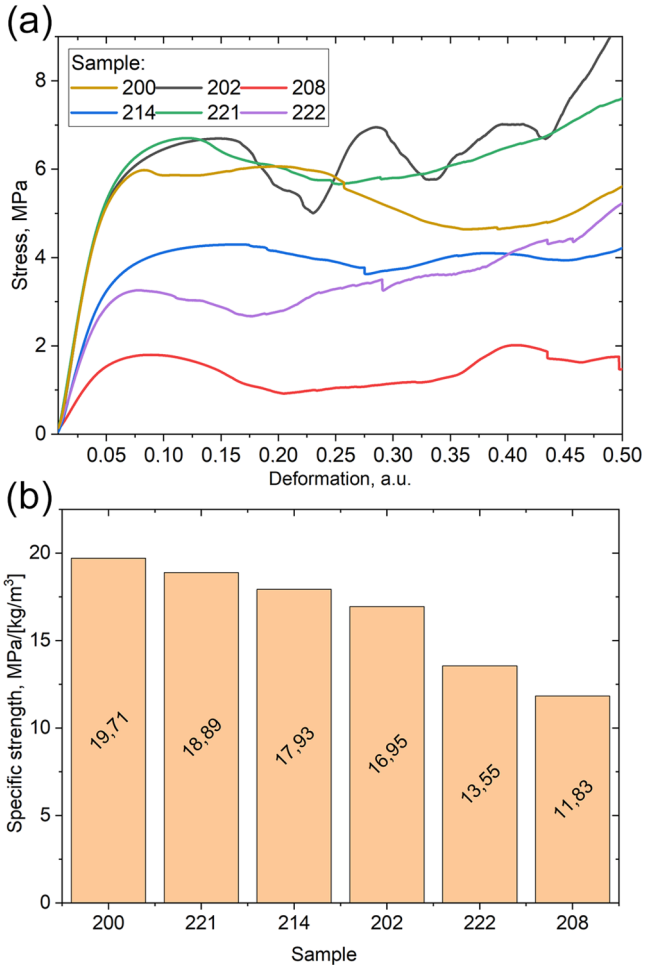

Figure 4. (a) Experimental deformation curves and (b) histogram of the specific strength of six 3D-printed cellular samples.

It can be seen that the transition to the plastic region is performed for all samples at 4% strain, which corresponds to a compression of 1.2 mm. The sample on the basis of the crystal structure from space group #202 has a distinctive curve, which can be interpreted as follows: when the ultimate strength is reached, there is a sharp decrease in the load associated with the fluidity of the cellular layer. As soon as one layer has completely collapsed (the first minimum on the curve), the material has partially compacted and is able to continue to resist the load. A similar behavior is observed for the second and third layers. As soon as complete compaction occurs, a gradual increase in stress occurs. The same interpretation also works for other samples, where, taking into account the

https://doi.org/10.1021/acsomega.3c00874
ACS Omega 2023, 8, 24865−24874

Table 4. Comparison among the Designed Relative Densities, Weighted Relative Densities, and Array Size for the Complex Geometries[a]

space group #	size (mm)	weight (g) 1	2	3	designed relative density (%)
200	30 ± 0.1	8.2	8.1	8.3	30
202		11.2	10.4	10.3	39
208		4	3.9	4.1	15
214		6.4	6.8	6.5	24
221		9.3	9.5	8.9	34
222		7.8	8.1	7.3	29

[a]All cubes are designed to have 30 mm sides.

characteristics of the sample, another characteristic curve is observed.

In addition, it was found that the dependence of the relative strength vs relative density of our samples obeys the Gibson–Ashby law[60] (Figure 5). The relative strength here means the

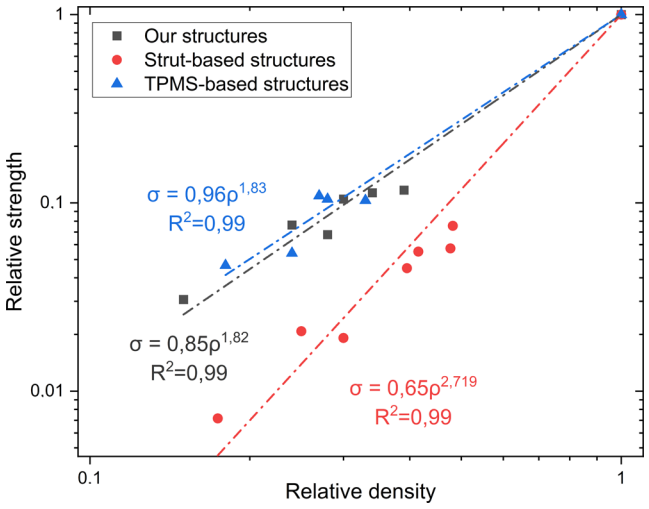

Figure 5. Relative strength Ashby charts of our samples in comparison to that of TPMS-[62] and strut-based[61] lattices.

ratio of the strength of the cellular material to the strength of the solid material. It can be seen from Figure 5 that the error of the linear approximation is small. The parameters of the obtained samples were compared with the parameters of several experimental works found in the literature.[61,62] Khiavi et al.[61] studied the mechanical properties of PA12 strut-based cellular materials. Shevchenko et al.[62] studied the mechanical properties of PA12 TPMS-based cellular materials. Additionally, it also follows from Figure 5 that the approximating lines for our structures and materials based on TPMS are close to each other, which allows us to conclude that using the "crystallomorphic design" it is possible to obtain a TPMS-like topology. In general, sheet-based cellular structures (ours and TPMS) have superior mechanical properties compared to strut-based cellular materials.

The values of the specific strength in relation to the filling factor from Table 4, which takes into account the weight of the product, are presented in Figure 4b.

As a result, the most durable, considering the weight of the material, is the 200 sample from the space group #200 with an IWP-like topology. The sample from s.g. #208 turned out to be less durable. Among the structures with a new unique topology, the 221 sample can be distinguished.

In accordance with eq 3, impact absorption energy A was determined at 30% deformation. The results are presented in Table 5.

Table 5. Energy-Absorbing Properties of the Samples

	space group # 200	221	214	202	222	208
A (MJ/m^3)	1.57	1.65	1.07	1.67	0.84	0.37

Samples 200, 221, and 202 can be singled out as the most preferred structures in terms of mechanical energy dissipation (Figure 6a, Table 5). Among the studied samples, the 221 sample has a preferred combination of high strength, efficiency, and energy-absorbing properties.

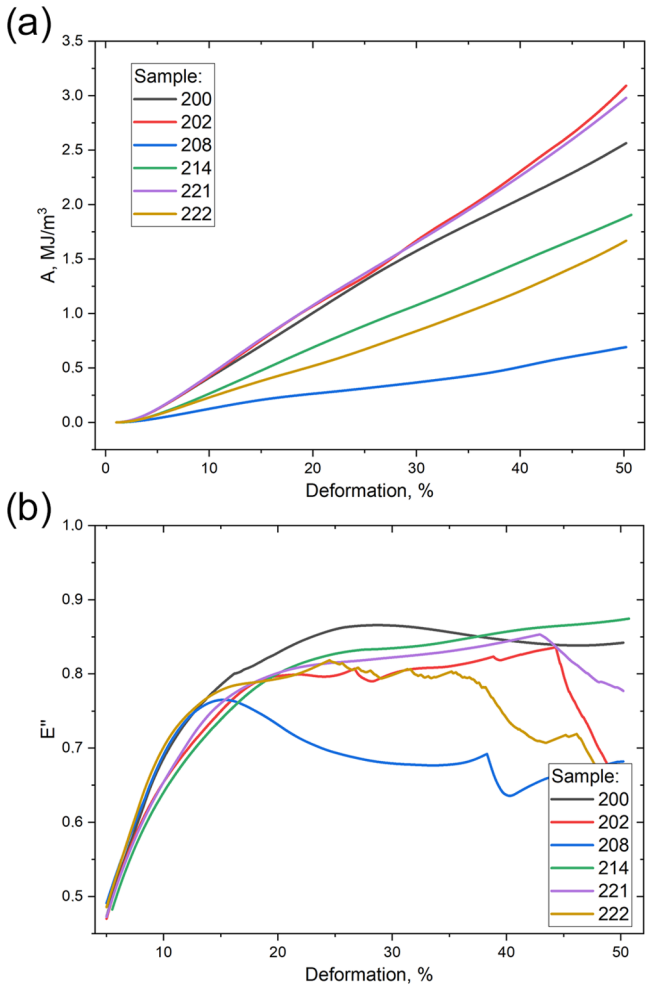

Figure 6. (a) Dependence of impact absorption energy and (b) effective impact absorption energy on deformation of the samples.

It can be seen that the graph of the specific impact absorption energy from deformation for all samples is almost linear, which indicates the uniformity of energy absorption during deformation of the samples under the action of external forces. Such energy absorption curves are characteristic of classic honeycomb materials used for single action energy absorbers.[63] Samples 200 and 202 absorb more energy when

https://doi.org/10.1021/acsomega.3c00874
ACS Omega 2023, 8, 24865−24874

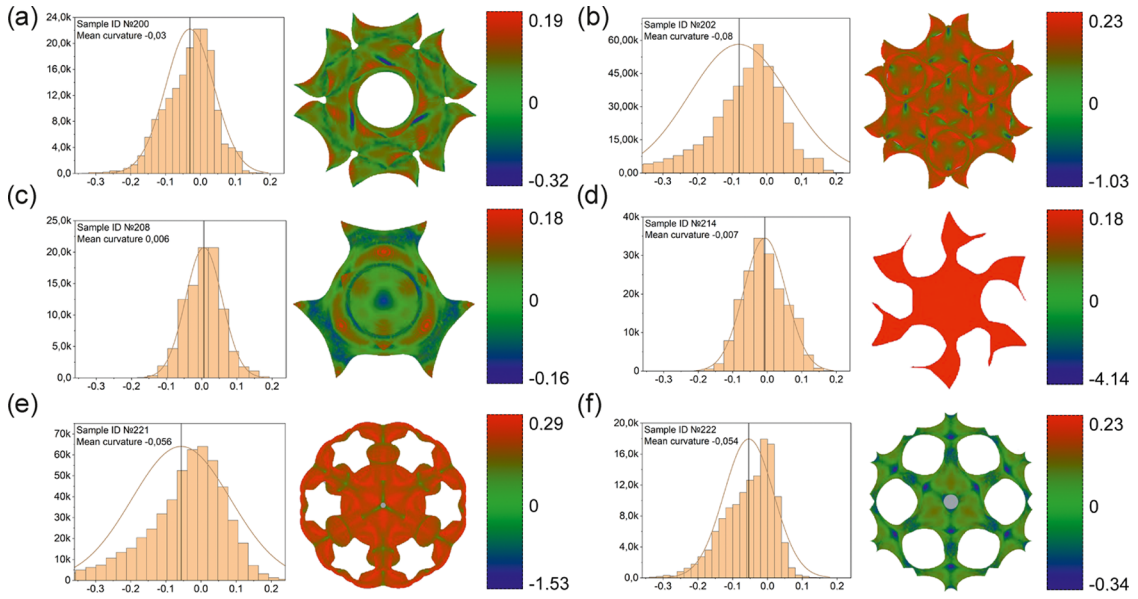

Figure 7. Mean curvature distributions, plotted as histograms and color-encoded surfaces, for the samples 200, 202, 208, 214, 221, and 222 (images a−f, respectively).

Table 6. Values of the Correlation of the Specific Strength and Parameters of the Crystal Structure

correlation of structure parameters with specific strength								
N_{nodes}	N_{bonds}	V (Å^3)	d_{min} (Å)	d_{max} (Å)	d_{avg} (Å)	φ_{min} (°)	φ_{max} (°)	φ_{avg} (°)
0.40	0.50	0.52	0.81	0.21	−0.58	0.87	0.56	−0.56

deformed than the other samples because the slope of the energy absorption curve of samples 200 and 202 is higher than that of the other samples.

To evaluate the shock-absorbing characteristics of cellular materials, it is convenient to use the effective impact absorption energy E''. For an ideal energy absorber, $E'' = 1$. All of the studied samples except for #208 have a high effective impact energy E'' (Figure 5b), and the maximum value of E'' for samples 200 and 214 exceeds 0.8, which is a high value.

In order to understand the difference in mechanical properties, some analytic approach should be used. For example, in paper,[64] skeletal graphs are used. Here, were implemented two approaches: (1) to estimate the mean curvature of the generatrix; and (2) possibly find the relationship between the parameters of the crystal cell used as a source for modeling and the strength of the derived samples.

3.4. Mean Surface Curvature. Let us consider the isosurface obtained for the #200 sample. Figure 7 shows the mean curvature distribution, which can be attributed to the Gaussian type (normal). Mathematical expectation of the mean curvature $\mu = -0.03$. The image shows that the surface does not contain areas of a sharp change of curvature values.

As a result, these surfaces are very close to minimal ones and they can be considered TPMS-like. For sample 208, the mean curvature is positive (Figure 7c), and it turned out to be weak (Figure 4b). Samples with mean curvature equal to 0 or a negative curvature show the best results.

3.5. Parameters of Crystalline Compounds. Further, it was assumed that mechanical properties should correlate with some parameters of crystalline compounds. The correlation coefficients of specific strength with values of studied parameters are shown in Table 6 and Figure 8. Here, N_{nodes} is the number of nodes; N_{bonds} is the number of bonds between atoms in the unit cell; d_{min}, d_{max}, and d_{avg} are the minimal, maximal, and average distances between nodes, respectively; φ_{min}, φ_{max}, and φ_{avg} are the minimal, maximal, and average angles between bonds in the structure simplified by the *ToposPro*[46] software package, respectively; and V is the cell volume.

From Table 6 and Figure 8, it follows that the highest correlation is observed for the minimum angle and the minimum bond length in the simplified crystal structures.

According to Table 5, sample #202 is the most energy-absorbing. Compared to the others, one can see that #200 has a large number of struts (ribs) (Figure 2c), so its specific strength is also higher. Similar strut-reinforced TPMS-based lattices were designed and tested in Cai's work.[65] From his results, it was found that for the case of a vertical ribbed structure, the effective uniaxial modulus of the primary primitive sheet-based TPMS structure can be significantly improved. Thus, independent of Cai's work, using our high-throughput screening approach, the cell-based arrays with a similar topology and high specific mechanical characteristics were found. This demonstrates the potential of the proposed approach in the search for new topologies of cellular materials with improved mechanical properties.

4. CONCLUSIONS

For the design of new high-strength cellular structures with increased energy-absorbing properties, a high-throughput approach has been developed. The method is based on extraction of structures of cubic zeolites from the extensive ATLAS database and processing them by the *ToposPro* software package. This made it possible to obtain complete statistics of cubic zeolites from the ATLAS database, which was

https://doi.org/10.1021/acsomega.3c00874
ACS Omega 2023, 8, 24865−24874

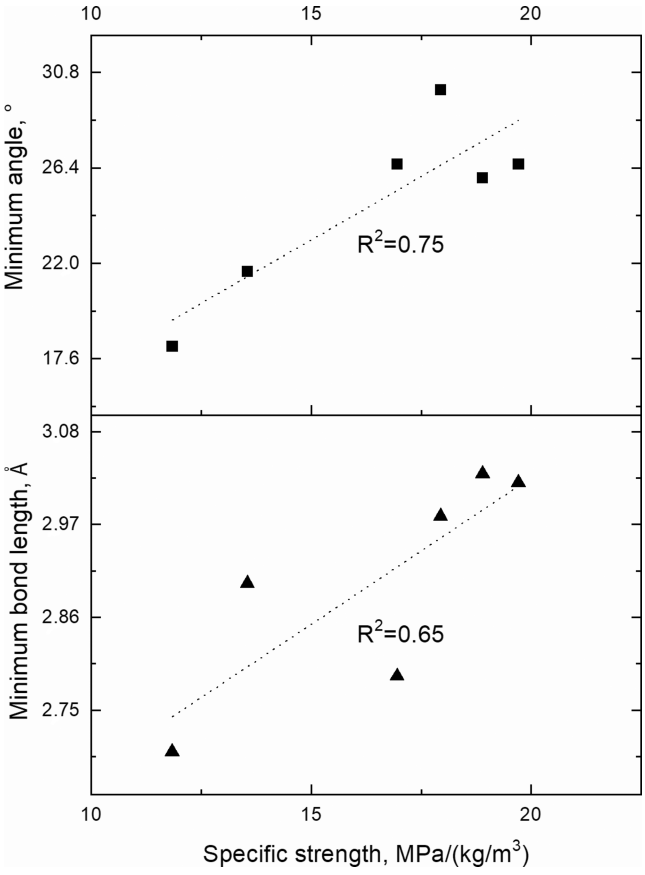

Figure 8. Correlation between the specific strength of the sample and minimum angle and minimum bond length in the simplified structures.

subsequently used in the study of correlations. The approach used in the work made it possible to find analogues of IWP and gyroid, which makes this technique promising for the search for new TPMS and TPMS-like structures. A study of the mechanical properties of thus-designed samples proved its validity. It is shown that specific strength has a linear correlation with the mean curvature. The surfaces of the structures under study do not contain areas with high positive/negative mean curvature, which means that the topology is TPMS-like, but not minimal. The study of the parameters of crystal structures, the isoelectronic surface of which is similar to that of TPMS, revealed the presence of a linear correlation between the strength of the sample and the number of atoms in the unit cell. The maximum correlation coefficient was found to be 0.87 (vs minimum angle in the simplified crystal structure). These findings allow one to predict the mechanical properties of cellular structures. A new cellular geometry with the structure reinforced by struts and increased strength and energy absorption was found, sample #202. This property was discovered by us independent of Cai's works,[60] in which the cellular structures were developed by a more explicit method. Our research demonstrates the potential of our approach in the design, screening, and prediction of mechanical characteristics of new TPMS-like cellular materials with superior performance.

■ ASSOCIATED CONTENT

Supporting Information

The Supporting Information is available free of charge at https://pubs.acs.org/doi/10.1021/acsomega.3c00874.

Details regarding the methodology of crystal chemical analysis using ToposPro: screening, simplification of the structures, identification of number of nodes, bonds, angles between bonds and bond lengths; histogram of distribution of zeolite structures by space group number; and results of crystal chemical analysis of some cube zeolites from the ATLAS database (PDF)

■ AUTHOR INFORMATION

Corresponding Author

Maxim Yu. Arsentev − *Institute of Silicate Chemistry, Russian Academy of Sciences, St. Petersburg 199034, Russia;* orcid.org/0000-0001-6166-4618; Email: ars21031960@gmail.com

Authors

Evgeny I. Sysoev − *Department of Micro- and Nanoelectronics, Saint Petersburg Electrotechnical University "LETI", St. Petersburg 197376, Russia;* orcid.org/0009-0002-6924-0427

Alexey I. Makogon − *Institute of Silicate Chemistry, Russian Academy of Sciences, St. Petersburg 199034, Russia*

Sergey V. Balabanov − *Institute of Silicate Chemistry, Russian Academy of Sciences, St. Petersburg 199034, Russia;* orcid.org/0000-0002-2249-350X

Maxim M. Sychev − *Institute of Silicate Chemistry, Russian Academy of Sciences, St. Petersburg 199034, Russia*

Mahmoud H. Hammouri − *Department of Physics, Natural and Applied Sciences, University of Wisconsin-Green Bay, Green Bay, Wisconsin 54311, United States*

Vyacheslav A. Moshnikov − *Department of Micro- and Nanoelectronics, Saint Petersburg Electrotechnical University "LETI", St. Petersburg 197376, Russia*

Complete contact information is available at: https://pubs.acs.org/10.1021/acsomega.3c00874

Notes

The authors declare no competing financial interest.

■ ACKNOWLEDGMENTS

Crystallographic analysis of structures from the ATLAS database and "crystallomorphic design" of samples was supported by the Russian Science Foundation (grant no. 20-73-10171). 3D printing and study of physical and mechanical properties of cellular structures are supported by the State Assignment for the Institute of Silicate Chemistry of the Russian Academy of Sciences (state registration number 0081-2022-0001).

■ REFERENCES

(1) Rashed, M. G.; Ashraf, M.; Mines, R. A. W.; Hazell, P. J. Metallic Microlattice Materials: A Current State of the Art on Manufacturing, Mechanical Properties and Applications. *Mater. Des.* **2016**, *95*, 518−533.

(2) Feng, J.; Fu, J.; Yao, X.; He, Y. Triply Periodic Minimal Surface (TPMS) Porous Structures: From Multi-Scale Design, Precise Additive Manufacturing to Multidisciplinary Applications. *Int. J. Extreme Manuf.* **2022**, *4*, No. 022001.

https://doi.org/10.1021/acsomega.3c00874
ACS Omega 2023, 8, 24865−24874

(3) Pasquale, G. D.; Tagliaferri, A. Modeling and Characterization of Mechanical and Energetic Elastoplastic Behavior of Lattice Structures for Aircrafts Anti-Icing Systems. *Proc. Inst. Mech. Eng., Part C* **2021**, *235*, 1828−1839.
(4) Maconachie, T.; Leary, M.; Lozanovski, B.; Zhang, X.; Qian, M.; Faruque, O.; Brandt, M. SLM Lattice Structures: Properties, Performance, Applications and Challenges. *Mater. Des.* **2019**, *183*, No. 108137.
(5) Oftadeh, R.; Perez-Viloria, M.; Villa-Camacho, J. C.; Vaziri, A.; Nazarian, A. Biomechanics and Mechanobiology of Trabecular Bone: A Review. *J. Biomech. Eng.* **2015**, *137*, No. 010802.
(6) Tiwary, C. S.; Kishore, S.; Sarkar, S.; Mahapatra, D. R.; Ajayan, P. M.; Chattopadhyay, K. Morphogenesis and Mechanostabilization of Complex Natural and 3D Printed Shapes. *Sci. Adv.* **2015**, *1*, No. e1400052.
(7) Peisker, H.; Michels, J.; Gorb, S. N. Evidence for a Material Gradient in the Adhesive Tarsal Setae of the Ladybird Beetle Coccinella Septempunctata. *Nat. Commun.* **2013**, *4*, No. 1661.
(8) Frazzetta, T. H. The Mechanics of Cutting and the Form of Shark Teeth (Chondrichthyes, Elasmobranchii). *Zoomorphology* **1988**, *108*, 93−107.
(9) Yoon, S.-H.; Park, S. A Mechanical Analysis of Woodpecker Drumming and Its Application to Shock-Absorbing Systems. *Bioinspiration Biomimetics* **2011**, *6*, No. 016003.
(10) Lee, Y.; Lim, Y.; Shin, H. Mixed-Scale Channel Networks Including Kingfisher-Beak-Shaped 3D Microfunnels for Efficient Single Particle Entrapment. *Nanoscale* **2016**, *8*, 11810−11817.
(11) Meza, L. R.; Das, S.; Greer, J. R. Strong, Lightweight, and Recoverable Three-Dimensional Ceramic Nanolattices. *Science* **2014**, *345*, 1322−1326.
(12) Meza, L. R.; Zelhofer, A. J.; Clarke, N.; Mateos, A. J.; Kochmann, D. M.; Greer, J. R. Resilient 3D Hierarchical Architected Metamaterials. *Proc. Natl. Acad. Sci. U.S.A.* **2015**, *112*, 11502−11507.
(13) Yuan, L.; Ding, S.; Wen, C. Additive Manufacturing Technology for Porous Metal Implant Applications and Triple Minimal Surface Structures: A Review. *Bioact. Mater.* **2019**, *4*, 56−70.
(14) Maskery, I.; Aboulkhair, N. T.; Aremu, A. O.; Tuck, C. J.; Ashcroft, I. A. Compressive Failure Modes and Energy Absorption in Additively Manufactured Double Gyroid Lattices. *Addit. Manuf.* **2017**, *16*, 24−29.
(15) Maskery, I.; Sturm, L.; Aremu, A. O.; Panesar, A.; Williams, C. B.; Tuck, C. J.; Wildman, R. D.; Ashcroft, I. A.; Hague, R. J. M. Insights into the Mechanical Properties of Several Triply Periodic Minimal Surface Lattice Structures Made by Polymer Additive Manufacturing. *Polymer* **2018**, *152*, 62−71.
(16) Al-Ketan, O.; Abu Al-Rub, R. K. Multifunctional Mechanical Metamaterials Based on Triply Periodic Minimal Surface Lattices. *Adv. Eng. Mater.* **2019**, *21*, No. 1900524.
(17) Yang, L.; Yan, C.; Han, C.; Chen, P.; Yang, S.; Shi, Y. Mechanical Response of a Triply Periodic Minimal Surface Cellular Structures Manufactured by Selective Laser Melting. *Int. J. Mech. Sci.* **2018**, *148*, 149−157.
(18) Yu, S.; Sun, J.; Bai, J. Investigation of Functionally Graded TPMS Structures Fabricated by Additive Manufacturing. *Mater. Des.* **2019**, *182*, No. 108021.
(19) Ambekar, R. S.; Oliveira, E. F.; Kushwaha, B.; Pal, V.; Machado, L. D.; Sajadi, S. M.; Baughman, R. H.; Ajayan, P. M.; Roy, A. K.; Galvao, D. S.; Tiwary, C. S. On the Mechanical Properties of Atomic and 3D Printed Zeolite-Templated Carbon Nanotube Networks. *Addit. Manuf.* **2021**, *37*, No. 101628.
(20) Shevchenko, V. Y.; Sychev, M. M.; Lapshin, A. E.; Lebedev, L. A. Ceramic Materials with the Triply Periodic Minimal Surface for Constructions Functioning under Conditions of Extreme Loads. *Glass Phys. Chem.* **2017**, *43*, 605−607.
(21) Shevchenko, V. Y.; Sychev, M. M.; Lapshin, A. E.; Lebedev, L. A.; Gruzdkov, A. A.; Glezer, A. M. Polymer Structures with the Topology of Triply Periodic Minimal Surfaces. *Glass Phys. Chem.* **2017**, *43*, 608−610.
(22) Winter, B.; Butz, B.; Dieker, C.; Schröder-Turk, G. E.; Mecke, K.; Spiecker, E. Coexistence of Both Gyroid Chiralities in Individual Butterfly Wing Scales of Callophrys Rubi. *Proc. Natl. Acad. Sci. U.S.A.* **2015**, *112*, 12911−12916.
(23) Luzzati, V.; Tardieu, A.; Gulik-Krzywicki, T.; Rivas, E.; Reiss-Husson, F. Structure of the Cubic Phases of Lipid−Water Systems. *Nature* **1968**, *220*, 485−488.
(24) Barois, P.; Hyde, S.; Ninham, B.; Dowling, T. Observation of Two Phases within the Cubic Phase Region of a Ternary Surfactant Solution. *Langmuir* **1990**, *6*, 1136−1140.
(25) Larsson, M.; Larsson, K.; Andersson, S.; Kakhar, J.; Nylander, T.; Ninham, B.; Wollmer, P. The alveolar surface structure: transformation from a liposome-like dispersion into a tetragonal CLP bilayer phase. *J. Dispersion Sci. Technol.* **1999**, *20*, 1−12.
(26) Kresge, C. T.; Leonowicz, M. E.; Roth, W. J.; Vartuli, J. C.; Beck, J. S. Ordered Mesoporous Molecular Sieves Synthesized by a Liquid-Crystal Template Mechanism. *Nature* **1992**, *359*, 710−712.
(27) Von Schnering, H. G.; Nesper, R. The Curvature of Chemical Structures. *J. Phys. Colloq.* **1990**, *51*, C7-383−C7-396.
(28) Sun, J.; Bonneau, C.; Cantín, Á.; Corma, A.; Díaz-Cabañas, M. J.; Moliner, M.; Zhang, D.; Li, M.; Zou, X. The ITQ-37 Mesoporous Chiral Zeolite. *Nature* **2009**, *458*, 1154−1157.
(29) Braun, E.; Lee, Y.; Moosavi, S. M.; Barthel, S.; Mercado, R.; Baburin, I. A.; Proserpio, D. M.; Smit, B. Generating Carbon Schwarzites via Zeolite-Templating. *Proc. Natl. Acad. Sci. U.S.A.* **2018**, *115*, E8116−E8124.
(30) Gaal, V.; Felix, L. C.; Woellner, C. F.; Galvao, D. S.; Tiwary, C. S.; D'Ávila, M. A.; Rodrigues, V. Mechanical Properties of 3D Printed Macroscopic Models of Schwarzites. *Nano Sel.* **2022**, *3*, 450−458.
(31) Li, X.; Yu, X.; Chua, J. W.; Lee, H. P.; Ding, J.; Zhai, W. Microlattice Metamaterials with Simultaneous Superior Acoustic and Mechanical Energy Absorption. *Small* **2021**, *17*, No. 2100336.
(32) Felix, L. C.; Ambekar, R. S.; Woellner, C. F.; Kushwaha, B.; Pal, V.; Tiwary, C. S.; Galvao, D. S. Mechanical Properties of 3D-Printed Pentadiamond. *J. Phys. D: Appl. Phys.* **2022**, *55*, No. 465301.
(33) Woodcock, L. V. Entropy Difference between the Face-Centred Cubic and Hexagonal Close-Packed Crystal Structures. *Nature* **1997**, *385*, 141−143.
(34) Libonati, F.; Graziosi, S.; Ballo, F.; Mognato, M.; Sala, G. 3D-Printed Architected Materials Inspired by Cubic Bravais Lattices. *ACS Biomater. Sci. Eng.* **2021**, No. 0c01708.
(35) Sajadi, S. M.; Woellner, C. F.; Ramesh, P.; Eichmann, S. L.; Sun, Q.; Boul, P. J.; Thaemlitz, C. J.; Rahman, M. M.; Baughman, R. H.; Galvão, D. S.; et al. 3D Printed Tubulanes as Lightweight Hypervelocity Impact Resistant Structures. *Small* **2019**, *15*, No. 1904747.
(36) Sajadi, S. M.; Owuor, P. S.; Schara, S.; Woellner, C. F.; Rodrigues, V.; Vajtai, R.; Lou, J.; Galvão, D. S.; Tiwary, C. S.; Ajayan, P. M. Multiscale Geometric Design Principles Applied to 3D Printed Schwarzites. *Adv. Mater.* **2018**, *30*, No. 1704820.
(37) Mackay, A. L.; Terrones, H. Diamond from Graphite. *Nature* **1991**, *352*, 762.
(38) Baughman, R. H.; Galvão, D. S. Crystalline Networks with Unusual Predicted Mechanical and Thermal Properties. *Nature* **1993**, *365*, 735−737.
(39) Felix, L. C.; Gaál, V.; Woellner, C. F.; Rodrigues, V.; Galvao, D. S. Mechanical Properties of Diamond Schwarzites: From Atomistic Models to 3D-Printed Structures. *MRS Adv.* **2020**, *5*, 1775−1781.
(40) Gibson, L. J. Cellular Solids. *MRS Bull.* **2003**, *28*, 270−274.
(41) Ashby, M. The Properties of Foams and Lattices. *Philos. Trans. R. Soc., A* **2006**, *364*, 15−30.
(42) Treacy, M. M. J.; Rao, S.; Rivin, I. *A Combinatorial Method for Generating New Zeolite Frameworks*, Proceedings from the Ninth International Zeolite Conference; Elsevier, 1993; pp 381−388 DOI: 10.1016/B978-1-4832-8383-8.50044-1.
(43) Akporiaye, D. E.; Price, G. D. Systematic Enumeration of Zeolite Frameworks. *Zeolites* **1989**, *9*, 23−32.

https://doi.org/10.1021/acsomega.3c00874
ACS Omega 2023, 8, 24865−24874

(44) Deem, M. W.; Newsam, J. M. Determination of 4-Connected Framework Crystal Structures by Simulated Annealing. *Nature* **1989**, *342*, 260−262.
(45) Gandhi, A.; Hasan, M. M. F. Machine Learning for the Design and Discovery of Zeolites and Porous Crystalline Materials. *Curr. Opin. Chem. Eng.* **2022**, *35*, No. 100739.
(46) Blatov, V. A.; Shevchenko, A. P.; Proserpio, D. M. Applied Topological Analysis of Crystal Structures with the Program Package ToposPro. *Cryst. Growth Des.* **2014**, *14*, 3576−3586.
(47) Wickham, H. *Ggplot2*; Springer New York: New York, NY, 2009 https://doi.org/10.1007/978-0-387-98141-3.
(48) Hohenberg, P.; Kohn, W. Inhomogeneous Electron Gas. *Phys. Rev.* **1964**, *136*, B864−B871.
(49) Kohn, W.; Sham, L. J. Self-Consistent Equations Including Exchange and Correlation Effects. *Phys. Rev.* **1965**, *140*, A1133−A1138.
(50) Waasmaier, D.; Kirfel, A. New Analytical Scattering-Factor Functions for Free Atoms and Ions. *Acta Crystallogr., Sect. A: Found. Crystallogr.* **1995**, *51*, 416−431.
(51) Momma, K.; Izumi, F. VESTA 3 for Three-Dimensional Visualization of Crystal, Volumetric and Morphology Data. *J. Appl. Crystallogr.* **2011**, *44*, 1272−1276.
(52) Yuan, S.; Chua, C. K.; Zhou, K. 3D-Printed Mechanical Metamaterials with High Energy Absorption. *Adv. Mater. Technol.* **2019**, *4*, No. 1800419.
(53) Chen, X.; Hu, M.; Sun, Y.; Yang, J.; Bai, L.; Xiong, Y. Wide-Range Tuning of the Mechanical Properties of TPMS Lattice Structures through Frequency Variation. *Mater. Des.* **2022**, *224*, No. 111370.
(54) Al-Ketan, O.; Rowshan, R.; Abu Al-Rub, R. K. Topology-Mechanical Property Relationship of 3D Printed Strut, Skeletal, and Sheet Based Periodic Metallic Cellular Materials. *Addit. Manuf.* **2018**, *19*, 167−183.
(55) Fan, X.; Tang, Q.; Feng, Q.; Ma, S.; Song, J.; Jin, M.; Guo, F.; Jin, P. Design, Mechanical Properties and Energy Absorption Capability of Graded-Thickness Triply Periodic Minimal Surface Structures Fabricated by Selective Laser Melting. *Int. J. Mech. Sci.* **2021**, *204*, No. 106586.
(56) Naghavi, S. A.; Tamaddon, M.; Marghoub, A.; Wang, K.; Babamiri, B. B.; Hazeli, K.; Xu, W.; Lu, X.; Sun, C.; Wang, L.; et al. Mechanical Characterisation and Numerical Modelling of TPMS-Based Gyroid and Diamond Ti6Al4V Scaffolds for Bone Implants: An Integrated Approach for Translational Consideration. *Bioengineering* **2022**, *9*, 504.
(57) Fogden, A.; Hyde, S. T. Parametrization of Triply Periodic Minimal Surfaces. I. Mathematical Basis of the Construction Algorithm for the Regular Class. *Acta Crystallogr., Sect. A: Found. Crystallogr.* **1992**, *48*, 442−451.
(58) Lodder, J. Curvature in the Calculus Curriculum. *Am. Math. Mon.* **2003**, *110*, 593−605.
(59) von Schnering, H. G.; Nesper, R. How Nature Adapts Chemical Structures to Curved Surfaces. *Angew. Chem., Int. Ed.* **1987**, *26*, 1059−1080.
(60) Gibson, L. J. Cellular Solids. *MRS Bull.* **2003**, *28*, 270−274.
(61) Ghaemi Khiavi, S.; Mohammad Sadeghi, B.; Divandari, M. Effect of Topology on Strength and Energy Absorption of PA12 Non-Auxetic Strut-Based Lattice Structures. *J. Mater. Res. Technol.* **2022**, *21*, 1595−1613.
(62) Shevchenko, V.; Balabanov, S.; Sychov, M.; Karimova, L. Prediction of Cellular Structures Mechanical Properties with the Geometry of Triply Periodic Minimal Surfaces (TPMS) *ACS Omega*.
(63) Mohammadi, H.; Ahmad, Z.; Petrů, M.; Mazlan, S. A.; Faizal Johari, M. A.; Hatami, H.; Rahimian Koloor, S. S. An Insight from Nature: Honeycomb Pattern in Advanced Structural Design for Impact Energy Absorption. *J. Mater. Res. Technol.* **2023**, *22*, 2862−2887.
(64) Sychov, M. M.; Lebedev, L. A.; Dyachenko, S. V.; Nefedova, L. A. Mechanical Properties of Energy-Absorbing Structures with Triply Periodic Minimal Surface Topology. *Acta Astronaut.* **2018**, *150*, 81−84.
(65) Cai, J.; Ma, Y.; Deng, Z. On the Effective Elastic Modulus of the Ribbed Structure Based on Schwarz Primitive Triply Periodic Minimal Surface. *Thin-Walled Struct.* **2022**, *170*, No. 108642.

https://doi.org/10.1021/acsomega.3c00874
ACS Omega 2023, 8, 24865−24874